Red-Light-Responsive Metallopolymer Nanocarriers with Conjugated and Encapsulated Drugs for Phototherapy Against Multidrug-Resistant Tumors

Mingjia Chen, Ningqiang Gong, Wen Sun, Jianxiong Han, Yuanli Liu, Shouwen Zhang, Aiping Zheng, Hans-Jürgen Butt, Xing-Jie Liang,* and Si Wu*

It is challenging to treat multidrug-resistant tumors because such tumors are resistant to a broad spectrum of structurally and functionally unrelated drugs. Herein, treatment of multidrug-resistant tumors using red-light-responsive metallopolymer nanocarriers that are conjugated with the anticancer drug chlorambucil (CHL) and encapsulated with the anticancer drug doxorubicin (DOX) is reported. An amphiphilic metallopolymer PolyRuCHL that contains a poly(ethylene glycol) (PEG) block and a red-light-responsive ruthenium (Ru)-containing block is synthesized. Chlorambucil is covalently conjugated to the Ru moieties of PolyRuCHL. Encapsulation of DOX into PolyRuCHL in an aqueous solution results in DOX@PolyRuCHL micelles. The DOX@PolyRuCHL micelles are efficiently taken up by the multidrug-resistant breast cancer cell line MCF-7R and which carries DOX into the cells. Free DOX, without the nanocarriers, is not taken up by MCF-7R or pumped out of MCF-7R via P-glycoproteins. Red light irradiation of DOX@PolyRuCHL micelles triggers the release of chlorambucil-conjugated Ru moieties and DOX. Both act synergistically to inhibit the growth of multidrug-resistant cancer cells. Furthermore, the inhibition of the growth of multidrug-resistant tumors in a mouse model using DOX@PolyRuCHL micelles is demonstrated. The design of red-light-responsive metallopolymer nanocarriers with both conjugated and encapsulated drugs opens up an avenue for photoactivated chemotherapy against multidrug-resistant tumors.

1. Introduction

Multidrug resistance is the simultaneous resistance of a cell to a broad spectrum of structurally and functionally unrelated chemotherapeutic drugs.[1] Multidrug resistance easily causes the failure of anticancer chemotherapy.[2] Multidrug-resistant tumor cells evolve two main pathways to deactivate drugs. In the first deactivation pathway, multidrug-resistant tumor cells overexpress efflux transporters such as P-glycoproteins,[3] which inhibit the uptake of drugs and pump drugs out of tumor cells.[4] To avoid this deactivation pathway, nanocarriers have been designed to decrease the efflux of drugs by P-glycoproteins[5] and to increase the uptake and accumulation of drugs in tumor cells.[6–13] For example, supramolecular micelles of amphiphilic dendrimers loaded with the anticancer agent doxorubicin (DOX) significantly promoted the intracellular drug concentration and inhibited tumor growth in a resistant tumor model.[14] In the second

M. Chen, W. Sun, J. Han, H.-J. Butt, S. Wu
Max Planck Institute for Polymer Research
Ackermannweg 10, 55128 Mainz, Germany
E-mail: wusi@mpip-mainz.mpg.de

N. Gong, X.-J. Liang
CAS Center for Excellence in Nanoscience and CAS Key Laboratory for Biological Effects of Nanomaterials and Nanosafety
National Center for Nanoscience and Technology
Chinese Academy of Sciences
Beijing 100190, China
E-mail: liangxj@nanoctr.cn

W. Sun
State Key Laboratory of Fine Chemicals
Dalian University of Technology
2 Linggong Road, Dalian 116024, China

Y. Liu
College of Materials Science and Engineering
Guilin University of Technology
Guilin 541004, China

S. Zhang
Neurophysiology Department
Beijing ChaoYang Emergency Medical Center
Beijing 100122, China

A. Zheng
Institute of Pharmacology and Toxicology of Academy of Military Medical Sciences
27 Taiping Road, Haidian District, Beijing 100850, China

S. Wu
CAS Key Laboratory of Soft Matter Chemistry
Anhui Key Laboratory of Optoelectronic Science and Technology
Department of Polymer Science and Engineering
University of Science and Technology of China
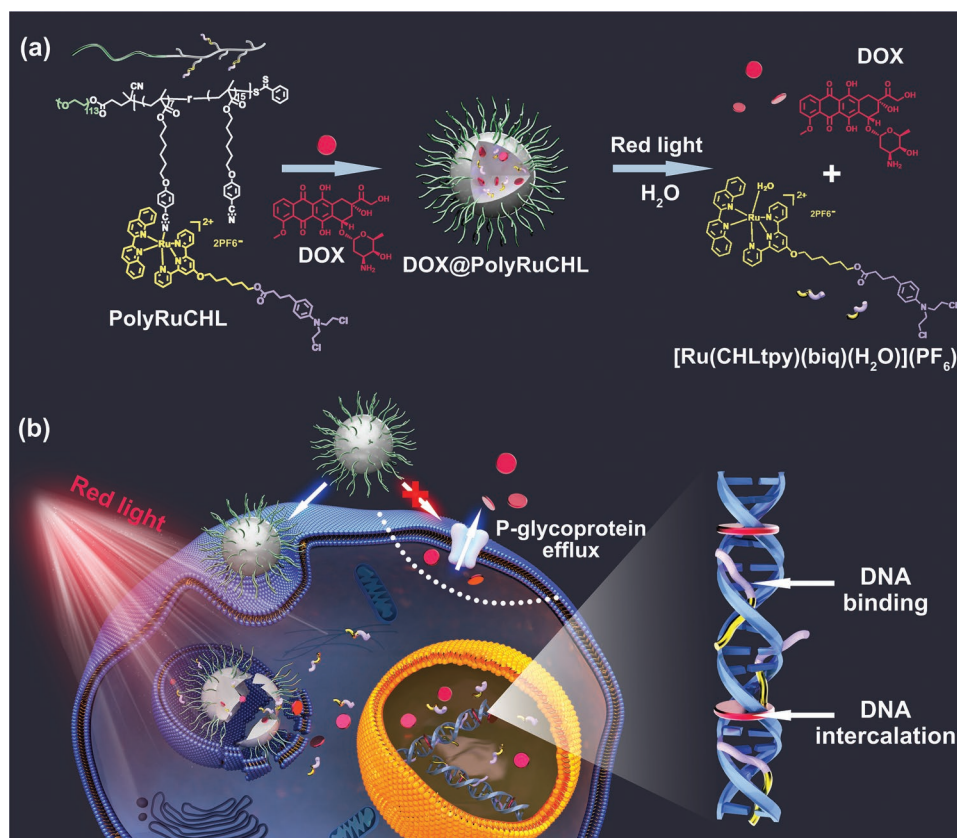Hefei 230026, China
E-mail: siwu@ustc.edu.cn

ADVANCED
SCIENCE NEWS

www.advancedsciencenews.com

NANO · MICRO

small

www.small-journal.com

Figure 1. a) Structures of PolyRuCHL, DOX, and [Ru(CHLtpy)(biq)(H₂O)](PF₆)₂. The compositions in the drug release system are illustrated using different colors. In particular, red round discs represent DOX. PolyRuCHL and DOX coassemble into DOX@PolyRuCHL micelles in an aqueous solution. Red light irradiation causes the release of DOX and [Ru(CHLtpy)(biq)(H₂O)](PF₆)₂. b) Inhibition of multidrug-resistant cancer cells using DOX@PolyRuCHL micelles. DOX@PolyRuCHL micelles are taken up by cancer cells via endocytosis. Red light irradiation of the DOX@PolyRuCHL micelles in the cells results in the release of DOX and [Ru(CHLtpy)(biq)(H₂O)](PF₆)₂, both of which damage the DNA of the cancer cells. In contrast, free DOX is ineffective in multidrug-resistant cancer cells because it is pumped out of the cell by P-glycoproteins.

deactivation pathway, multidrug-resistant tumor cells exhibit enhanced DNA repair capacity because they exacerbate the activity of excision repair cross-complementing proteins after tumor cell DNA damage, which avoids the apoptosis of tumor cells.[15] To prevent the second deactivation pathway, some anticancer agents were rationally combined for therapy, which resulted in synergistic effects.[16] For example, two drugs with different action mechanisms efficiently inhibited tumor growth.[17] Although strategies to prevent an individual deactivation pathway in multidrug-resistant cancer cells exist, it is a challenge to reverse multidrug resistance. Therefore, it is highly desirable to develop new strategies to overcome multiple deactivation pathways in multidrug-resistant cancer cells.

Here, we demonstrate the inhibition of multidrug-resistant tumors using red-light-responsive metallopolymer nanocarriers that are conjugated with the anticancer agent chlorambucil (CHL) and encapsulated with the anticancer agent DOX (**Figure 1**). The metallopolymer PolyRuCHL contains a hydrophilic poly(ethylene glycol) (PEG) block and a hydrophobic ruthenium (Ru)-containing block (Figure 1a). We designed a Ru-containing block to construct photoactivable

nanocarriers.[18–22] The Ru moieties can be cleaved from the polymer by red light.[23–25] Red light has the advantage that it can penetrate deeply into tissue for phototherapy.[26] Some Ru complexes have anticancer activities and are already in clinical trials.[27] Photocleavage of Ru complexes can generate cytotoxic Ru moieties or ligands for photoactivated chemotherapy.[28,29] Chlorambucil as the anticancer drug is conjugated to the Ru moieties of PolyRuCHL to enhance the anticancer activity. Moreover, DOX-encapsulated micelles DOX@PolyRuCHL were prepared by coassembly of DOX and PolyRuCHL (Figure 1a). DOX@PolyRuCHL micelles can be efficiently taken up by the multidrug-resistant breast cancer cell line MCF-7R. As a result, DOX accumulates in the cancer cells. The use of DOX@PolyRuCHL solves the problem that free DOX is pumped out of the cells via P-glycoproteins (Figure 1b). Irradiating DOX@PolyRuCHL with red light induces the release of chlorambucil-conjugated Ru complexes and DOX, which have synergistic effects to inhibit the growth of multidrug-resistant cells. Another advantage of photoactivated chemotherapy using DOX@PolyRuCHL is that phototoxicity is only generated in the irradiated tumor tissue, which improves the therapeutic selectivity.

2. Results and Discussion

2.1. Preparation and Characterization of Red-Light-Responsive Metallopolymer Nanocarriers

PolyRuCHL was synthesized via grafting [Ru(CHLtpy)(biq)(H$_2$O)](PF$_6$)$_2$ (CHLtpy = 6-([2,2″:6″,2″″-terpyridin]-4′-yloxy)hexyl 4-(4-(bis(2-chloroethyl)amino)phenyl)butanoate, biq = 2,2′-biquinoline) to PEG-*b*-PCPH (poly(ethylene glycol)-*block*-poly(6-(4-cyanophenoxy) hexyl methacrylate) by cyano–Ru coordination (Figure S1, Supporting Information).[24] PolyRuCHL was characterized using ^{1}H NMR (Figure S2, Supporting Information). The molecular weight of PolyRuCHL was 20.3 kg mol^{-1}. Approximately 7 Ru moieties were in each polymer chain. The weight fraction of the Ru moieties in PolyRuCHL was ≈45%. The anticancer agent chlorambucil was conjugated to the Ru moieties to improve anticancer activity.

To prepare micelles, PolyRuCHL was dissolved in a good solvent (THF/DMF = 4/1, v/v). Water was added to the solution to trigger self-assembly. Then, the organic solvents were removed via dialysis. PolyRuCHL formed micelles because of its amphiphilic structure. The diameters of PolyRuCHL micelles measured by transmission electron microscopy (TEM) and dynamic light scattering (DLS) were 15 and 22 nm, respectively (**Figure 2**a,c). The TEM measurements were conducted in a dry state and the DLS measurements were in solution.

Therefore, the diameters in the two measurements were slight different.[30] PolyRuCHL was used as a nanocarrier to encapsulate DOX. Therefore, PolyRuCHL and DOX were dissolved in the THF/DMF mixture (3/2, v/v). DOX@PolyRuCHL micelles in aqueous solution were prepared by adding water and subsequently removing the organic solvents. The diameters of DOX@PolyRuCHL micelles measured by TEM and DLS were 22 and 27 nm, respectively (Figure 2b,c), which were larger than those of PolyRuCHL micelles. The increase in the diameter suggests that DOX was successfully encapsulated into PolyRuCHL micelles. The encapsulation of DOX induced the shift of the absorption band of the micelles, which confirmed the successful encapsulation of DOX (Figure S3, Supporting Information). The content of the encapsulated DOX in DOX@PolyRuCHL micelles measured by fluorescence spectroscopy was 14.8% (Figure S4, Supporting Information). The as-prepared DOX@PolyRuCHL micelles were dialyzed against saline (0.9% w/v NaCl, pH 7.4) solution for 9 h. The dialysate had no fluorescence, suggesting that free DOX was removed completely via dialysis and that the encapsulated DOX did not leak out (Figure S5, Supporting Information). The diameter of the DOX@PolyRuCHL micelles in water and saline did not change after incubation for 48 h, indicating that the micelles were stable (Figure S6, Supporting Information). We have demonstrated that the Ru-containing polymer assemblies were more stable than their low-molecular weight analogs under physiological
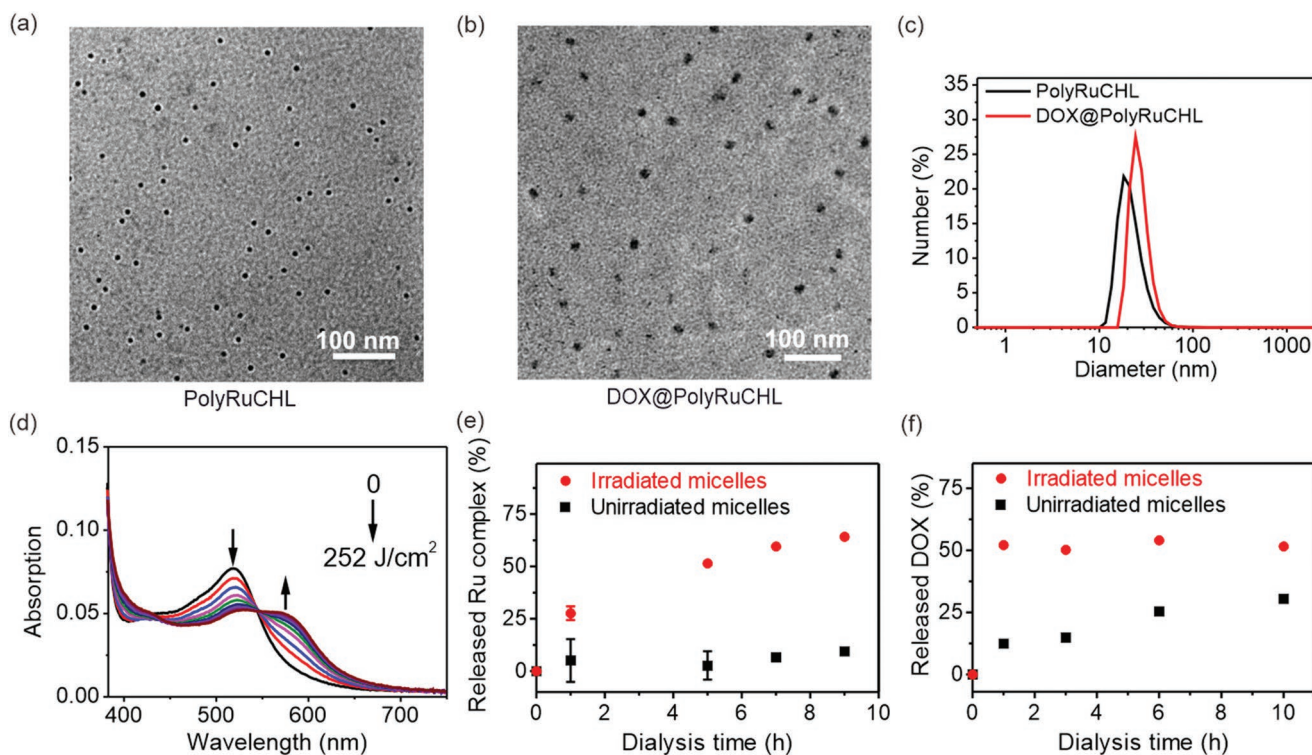

Figure 2. Transmission electron microscopy (TEM) images of a) PolyRuCHL micelles and b) DOX@PolyRuCHL micelles. c) Dynamic light scattering (DLS) data of PolyRuCHL and DOX@PolyRuCHL micelles in water. d) UV–vis absorption spectra of PolyRuCHL micelles in cell culture medium under 656 nm red light irradiation for different doses (from 0 to 252 J cm^{-2}). e) The release profiles of the Ru complex and f) the release profiles of DOX from the irradiated (656 nm, 270 J cm^{-2}) and unirradiated DOX@PolyRuCHL micelles measured using a dialysis device in a buffer solution (pH 5.5, 0.5% Tween-80). The released Ru complexes and DOX were quantified using inductively coupled plasma mass spectrometry (ICP-MS) and fluorescence spectroscopy, respectively.

**ADVANCED
SCIENCE NEWS**
www.advancedsciencenews.com

**NANO · MICRO
small**
www.small-journal.com

conditions by UV–vis absorption spectroscopy, which make them potential candidates for biomedical applications.[31]

PolyRuCHL micelles had a broad metal-to-ligand charge transfer (MLCT) band from ≈400 to ≈700 nm (Figure 2d). Visible light with different wavelengths could excite the MLCT band. Red light penetrates deeper into tissue than visible light with shorter wavelengths. For biomedical experiments, we used 656 nm red light in the therapeutic window (650–900 nm) to excite the micelles. The irradiation dose can accurately control photoreaction.[24] Red light irradiation induced a redshift of the MLCT band from 519 to 576 nm (Figure 2d). Such a change in the absorption spectra is the same as that of other Ru complexes that undergo ligand photosubstitution.[31–35] We also found that red light can activate Ru complexes after red light penetrates tissue with a thickness of up to 16 mm.[36] The absorption spectroscopy results showed that the chlorambucil-conjugated Ru moieties were photocleaved from the polymer.

We observed that red light irradiation of DOX@PolyRuCHL micelles in cell culture medium (Dulbecco's modified Eagle's medium, DMEM) promoted the co-release of [Ru(CHLtpy)(biq)-$(H_2O)](PF_6)_2$ and DOX (Figure 2e,f). The release is controlled by the irradiation dose (dose = power density × time). To quantify the amount of the released [Ru(CHLtpy)(biq)(H_2O)](PF_6)_2$ and DOX, DOX@PolyRuCHL micelles were irradiated with 656 nm red light (dose: 270 J cm^{-2}) and transferred to a mini dialyzer suspended in a buffer solution (pH 5.5, 0.5% Tween-80). The released [Ru(CHLtpy)(biq)(H_2O)](PF_6)_2$ and DOX were quantified using inductively coupled plasma mass spectrometry (ICP-MS) and fluorescence spectroscopy, respectively. Approximately 64% of the Ru moieties were detected in the dialysate after dialysis for 9 h (Figure 2e). In contrast, less than 10% of Ru moieties were detected when unirradiated DOX@PolyRuCHL micelles were used. In addition, when the irradiated DOX@PolyRuCHL micelles were dialyzed, more than 50% protonated DOX was quickly released, which was detected after dialysis within 1 h. The detected amount of DOX in the next 9 h remained unchanged (Figure 2f). In contrast, the DOX content gradually increased to 30% when the unirradiated DOX@PolyRuCHL micelles were dialyzed. We interpret that the release of DOX from the unirradiated DOX@PolyRuCHL micelles is because of the acidic environment (pH 5.5) of the dialysate protonated DOX and increased its water solubility. We observed the disassembly of PolyRuCHL micelles in the cell culture medium after red light irradiation, which should be the main reason for the red-light-induced co-release of [Ru(CHLtpy)(biq)-$(H_2O)](PF_6)_2$ and DOX (Figure S7, Supporting Information). The acidic environment also assisted the release of DOX.

2.2. Cellular Uptake and Anticancer Assessment in vitro

To test whether DOX@PolyRuCHL micelles can overcome the deactivation pathways that induce multidrug resistance, the multidrug-resistant breast cancer cell line MCF-7R was used in our study. Multidrug-resistant MCF-7R cells were incubated with free DOX (1.0×10^{-6} and 2.0×10^{-6} M), and cellular uptake of the drug was analyzed using flow cytometry. At 0.5 and 2 h post-incubation, limited enhancement of intracellular fluorescence was observed, suggesting that the uptake of free DOX by

MCF-7R cells was prohibited (**Figure 3**a,b). This is because the overexpressed P-glycoproteins on the cell membrane decreased the influx of DOX and pumped intracellular DOX out.[14] To further confirm the results, we measured the efflux of DOX from MCF-7R cells using flow cytometry (Figure 3c). Almost all free DOX was pumped out of the cells within 1 h, demonstrating that overexpressed P-glycoproteins caused the efflux of free DOX.

In contrast, MCF-7R cells incubated with DOX@PolyRuCHL (encapsulated DOX: 1.0×10^{-6} and 2.0×10^{-6} M) for 0.5 and 2 h showed significantly enhanced intracellular fluorescence (Figure 3a,b; Figure S8, Supporting Information). This result indicated that DOX@PolyRuCHL efficiently carried DOX into MCF-7R cells, which circumvented the efflux of DOX by P-glycoproteins. We found that enhancing DOX concentrations (from 1.0×10^{-6} to 2.0×10^{-6} M) and incubation time (from 0.5 to 2 h) can also enhance the cellular uptake of the drug, demonstrating that the endocytosis of DOX-encapsulated nanocarriers by MCF-7R cells occurred in both time- and concentration-dependent manners. We also used DOX@PolyRuCHL micelles to study the efflux of DOX (Figure 3c). The amount of DOX (delivered by DOX@PolyRuCHL micelles) in cells was nearly unchanged even after 4 h of incubation, which further demonstrated that DOX@PolyRuCHL micelles bypassed the deactivation pathway of the multidrug-resistant cells.

We investigated the cellular uptake mechanism of DOX@PolyRuCHL micelles via endocytosis inhibition. We used low temperature (4 °C) to inhibit energy-dependent cell uptake, NaN$_3$ was also used to inhibit energy-dependent cell uptake, and cytochalasin D (CD) was used to inhibit micropinocytosis (Figure 3d). The uptake was decreased by 47% at 4 °C and by 22% when using NaN$_3$, demonstrating that the endocytosis of DOX@PolyRuCHL micelles was an energy-dependent process.[5] The cellular uptake of DOX@PolyRuCHL micelles was only decreased by 6% when using CD, suggesting that the uptake of DOX@PolyRuCHL was not a macropinocytosis-mediated endocytosis.

The cellular uptake and the intracellular distribution of DOX and DOX@PolyRuCHL micelles were further studied using confocal laser scanning microscopy (CLSM) (Figure 3e). MCF-7R cells were incubated with free DOX for 270 min. Then, the cells were washed with phosphate-buffered saline (PBS) twice, stained with Hoechst 33 342, and imaged under CLSM (Figure 3e, column 2). Minimum fluorescence of DOX was observed in the cells, which demonstrated that free DOX was not taken up or was pumped out of the cells. In contrast, strong intracellular fluorescence of DOX was observed in the cytoplasm when MCF-7R cells were treated with DOX@PolyRuCHL micelles (Figure 3e, column 3). The internalization of DOX@PolyRuCHL micelles into cells was shown using lysosome co-localization (Figure S9, Supporting Information). The CLSM results together with the flow cytometry results confirmed that DOX@PolyRuCHL micelles efficiently carried DOX into multidrug-resistant cells. Thus, DOX@PolyRuCHL micelles overcame the deactivation pathway caused by overexpressed P-glycoproteins.

We then investigated whether red light irradiation can induce intracellular drug release. MCF-7R cells were incubated with DOX@PolyRuCHL micelles for 120 min. After that, the cells
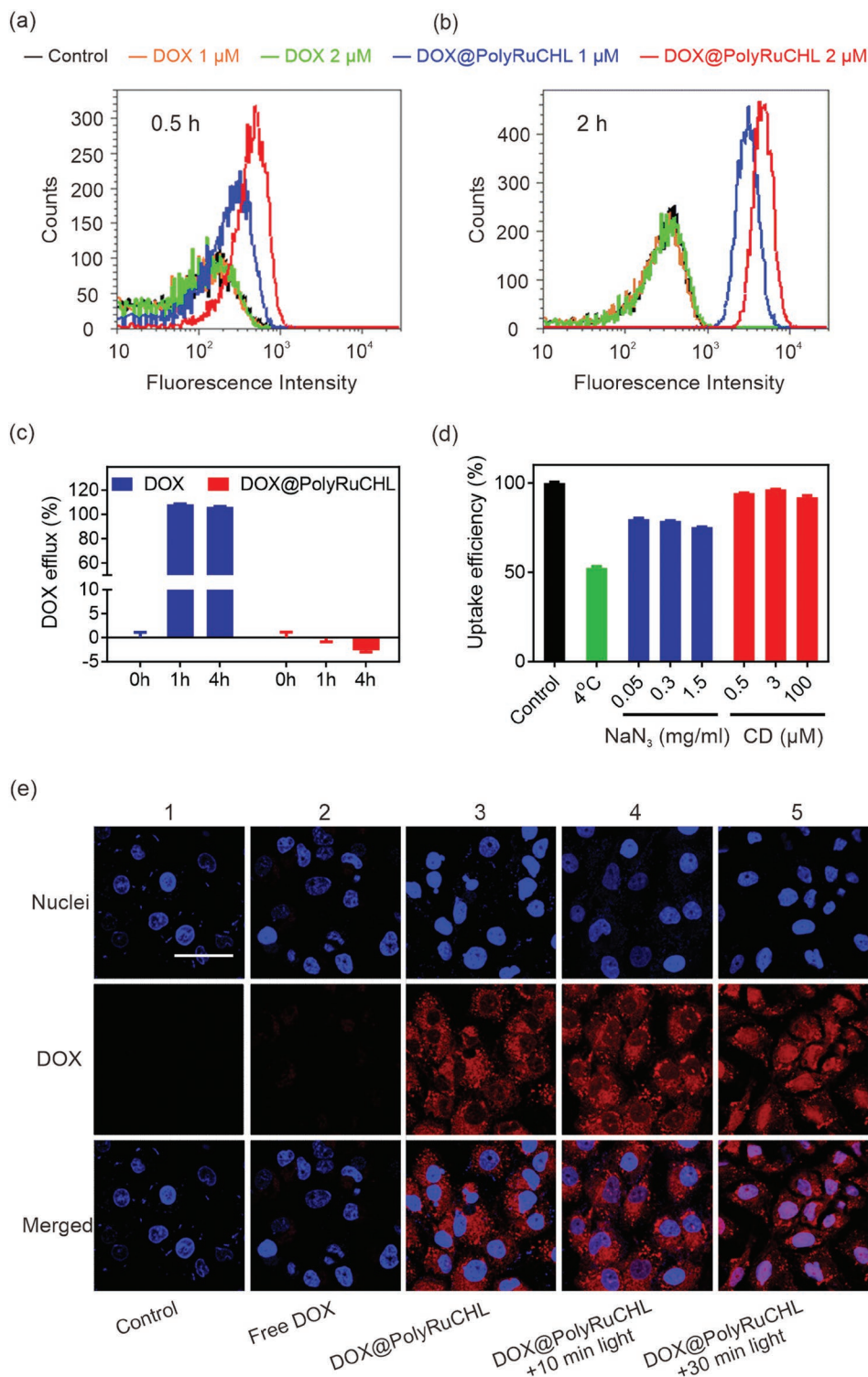
Figure 3. Flow cytometry results of drug-resistant MCF-7R cancer cells incubated with DOX@PolyRuCHL micelles (1×10^{-6} and 2×10^{-6} M) and free DOX (1×10^{-6} and 2×10^{-6} M) for a) 0.5 h and b) 2 h, respectively. c) The percentage of DOX efflux from drug-resistant MCF-7R cells that were incubated with free DOX and DOX@PolyRuCHL. d) The uptake of DOX@PolyRuCHL micelles by resistant MCF-7R cells under different endocytosis inhibition conditions for 1 h. 4 °C: inhibition of energy-dependent endocytosis; NaN₃: an inhibitor of ATP metabolites, inhibition of energy-dependent endocytosis; Cytochalasin D (CD): an inhibitor of micropinocytosis. e) Confocal laser scanning microscopy (CLSM) images of MCF-7R cells incubated with e-2) free DOX and e-3) DOX@PolyRuCHL micelles. After incubation for 120 min, MCF-7R cells with DOX@PolyRuCHL micelles were irradiated with a 660-nm laser for e-4) 10 min (30 J cm^{-2}), and e-5) 30 min (90 J cm^{-2}), respectively. The MCF-7R cells were subsequently incubated for another 140 and 120 min, respectively. The total incubation time of each group (including control group e-1) was the same (270 min). Nuclei were stained with Hoechst 33342 (blue). Red color represents the signal from DOX. Scale bar: 50 µm.

were irradiated with a 660-nm laser for 10 min (30 J cm^{-2}) and further incubated at 37 °C for 140 min (Figure 3e, column 4). Strong DOX fluorescence in the nuclei of MCF-7R cells was detected, demonstrating that DOX successfully entered cell nuclei. When we prolonged the irradiation time to 30 min (90 J cm^{-2}, i.e., kept the total incubation time the same), stronger DOX fluorescence in the cell nuclei was detected (Figure 3e, column 5). Although part of the released DOX could be pumped out of MCF-7R cells via P-glycoproteins, these CLSM images demonstrated that red light irradiation triggered intracellular drug release and that the released DOX accumulated at the nuclei.

We expect that the intracellularly released drugs can inhibit the growth of MCF-7R cells. Therefore, we measured the viability of MCF-7R cells incubated with DOX@PolyRuCHL micelles after red light irradiation using a cell counting kit-8 (CCK-8) assay (**Figure 4**a). The cell viability decreased as the concentration of DOX increased. The cell viability decreased to 22% with a concentration of DOX of 17.5 µg mL^{-1} for

DOX@PolyRuCHL. In comparison, free DOX at the same concentration did not efficiently inhibit the growth of MCF-7R cells.

To study the contributions of PolyRuCHL, encapsulated DOX, and light irradiation on the inhibition of cell growth, we compared the viability of MCF-7R cells in four groups: 1) light only, 2) DOX@PolyRuCHL, 3) PolyRuCHL + Light, and 4) DOX@PolyRuCHL+ Light (Figure 4b). DOX@PolyRuCHL or PolyRuCHL micelles were internalized by cells after incubation for 4 h and then irradiated with 656 nm red light (90 J cm^{-2}); the cells were further incubated for a total processing time of 24 h. For the light-only group, the cell viability was 93%, suggesting that light irradiation induced limited inhibition of cancer cell growth. For the DOX@PolyRuCHL group, the cell viability was 73% (DOX@PolyRuCHL concentration: 100 µg mL^{-1}). For the PolyRuCHL + Light group, the cell viability was 62% (PolyRuCHL concentration: 100 µg mL^{-1}), which can be explained by the released [Ru(CHLtpy)(biq)- (H$_2$O)](PF$_6$)$_2$ inducing toxicity to the cancer cells. The block copolymer without the [Ru(CHLtpy)(biq)(H$_2$O)](PF$_6$)$_2$ moiety
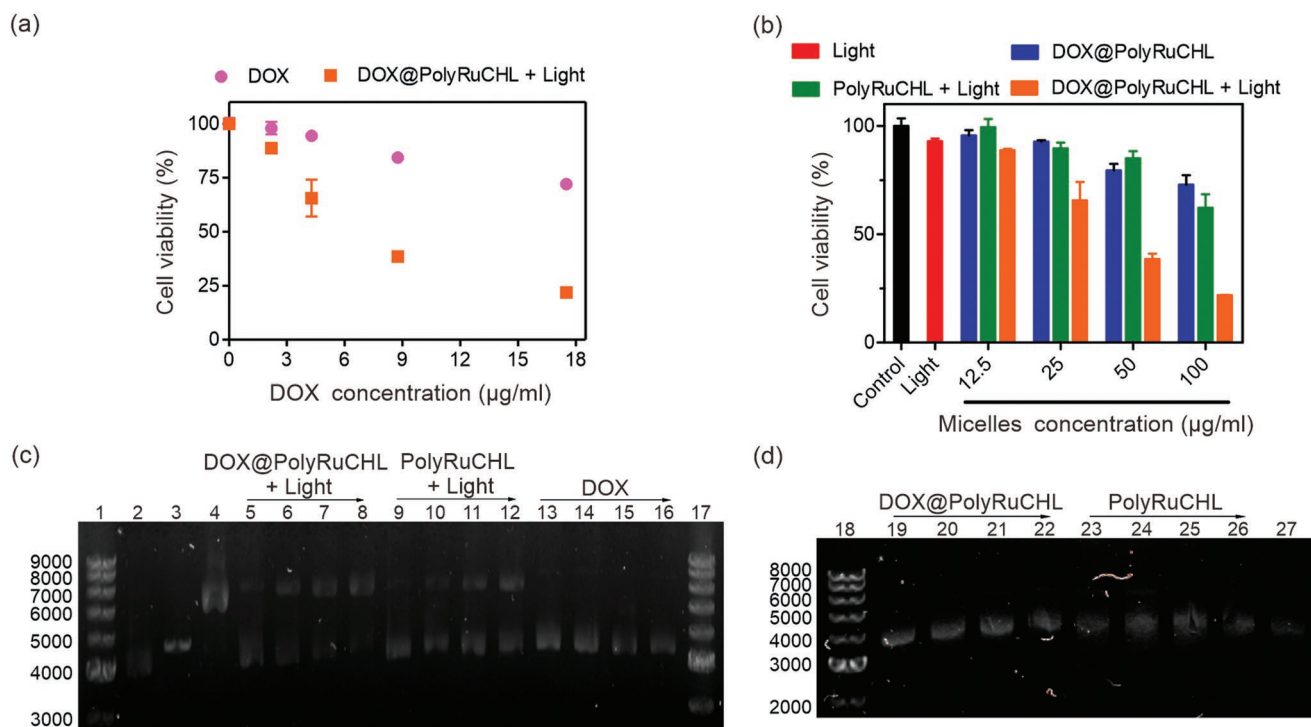

Figure 4. Viability of MCF-7R cells after different treatments: a) DOX group (pink): MCF-7R cells were incubated with free DOX; DOX@PolyRuCHL micelles + Light group (orange): MCF-7R cells were incubated with DOX@PolyRuCHL micelles for 4 h and irradiated with 656 nm red light (90 J cm^{-2}); b) Control group (black): MCF-7R cells were incubated without any treatment; Light group (red): MCF-7R cells were irradiated with 656 nm red light (90 J cm^{-2}); DOX@PolyRuCHL micelles group (blue): MCF-7R cells were incubated with DOX@PolyRuCHL micelles; PolyRuCHL micelles + Light group (green): MCF-7R cells were incubated with PolyRuCHL micelles for 4 h and irradiated with 656 nm red light (90 J cm^{-2}); DOX@PolyRuCHL micelles + Light group (orange): MCF-7R cells were incubated with DOX@PolyRuCHL micelles for 4 h and irradiated with 656 nm red light (90 J cm^{-2}). Cell viability was tested after incubation for 24 h. c) Agarose gel electrophoresis of the pUC19 plasmid (40 µg mL^{-1}) with different treatments. Lanes 1 and 17: DNA molecular weight standard; Lane 2: supercoiled DNA (≈4000 bp); Lane 3: linear DNA (≈5000 bp); Lane 4: relaxed circle DNA (≈6000 bp, Cu(phen)$_2$ reaction with supercoiled DNA); Lanes 5–8: supercoiled DNA incubated with 5, 20, 50, and 100 µg mL^{-1} DOX@PolyRuCHL micelles for 30 min and irradiated with 656 nm red light (180 J cm^{-2}); Lanes 9–12: supercoiled DNA incubated with 5, 20, 50, and 100 µg mL^{-1} PolyRuCHL micelles for 30 min and irradiated with 656 nm red light (180 J cm^{-2}); Lanes 13–16: supercoiled DNA incubated with 5, 10, 20, and 50 µg mL^{-1} DOX. The samples were incubated overnight after light irradiation before gel analysis. d) Agarose gel electrophoresis of the pUC19 plasmid (40 µg mL^{-1}) with different treatments in the dark. Lane 18: DNA molecular weight standard; Lane 27: supercoiled DNA (≈4000 bp); Lanes 19–22: supercoiled DNA incubated with 5, 20, 50, and 100 µg mL^{-1} DOX@PolyRuCHL micelles; Lanes 23–26: supercoiled DNA incubated with 5, 20, 50, and 100 µg mL^{-1} PolyRuCHL micelles. The samples were incubated overnight before gel analysis.

(PEG-*b*-CPH) showed no toxicity when its concentration reached 300 µg mL^{-1} (Figure S10, Supporting Information). The toxicity of [Ru(CHLtpy)(biq)(H$_2$O)](PF$_6$)$_2$ was improved after the anticancer agent CHL was conjugated to [Ru(tpy)(biq)(H$_2$O)](PF$_6$)$_2$ (Figure S11, Supporting Information). Remarkably, the cell viability for the DOX@PolyRuCHL+ Light group decreased to 22% (DOX@PolyRuCHL concentration: 100 µg mL^{-1}). The combination index of the co-released Ru complexes and DOX calculated by median-effect analysis was 0.69, which demonstrated that the co-released Ru complex [Ru(CHLtpy)(biq)(H$_2$O)](PF$_6$)$_2$ and DOX had a synergistic anticancer effect.

In the field of anticancer metallodrugs including Ru complexes, agarose gel electrophoresis is a standard method that is widely used to demonstrate DNA destruction.[37–39] To understand the mechanism of the synergistic anticancer effect, we investigated DNA damage caused by photoreleased [Ru(CHLtpy)(biq)(H$_2$O)](PF$_6$)$_2$ and DOX (Figure 4c,d). The DNA pUC19 plasmid was used as model DNA to evaluate the damage caused by the nanocarriers. Lanes 1 and 17 represented DNA ladder. Supercoiled DNA (≈4000 bp), linear DNA (≈5000 bp), and relaxed circle DNA (≈6000 bp) were in lanes 2, 3, and 4, respectively. After incubation with DOX (lanes 13–16, DOX concentration: 5, 10, 20, and 50 µg mL^{-1}), the plasmid DNA showed slightly decreased mobility compared to supercoiled DNA. This result suggested that DOX interacted with DNA by intercalation, which caused unwinding of the DNA.[40–42] After the pUC19 plasmid was incubated with PolyRuCHL micelles (lanes 9–12, micelle concentration: 5, 20, 50, and 100 µg mL^{-1}) and irradiated with red light (180 J cm^{-2}), the DNA showed decreased mobility in a dose-dependent manner. Moreover, the integrity of DNA adducts appeared above the relaxed circular DNA when the plasmid DNA was treated with DOX@PolyRuCHL+ Light (lanes 5–8, micelle concentration: 5, 20, 50, and 100 µg mL^{-1}; light dose: 180 J cm^{-2}). DNA was incubated with PolyRuCHL micelles (lanes 23–26, concentration: 5, 20, 50, and 100 µg mL^{-1}) or DOX@PolyRuCHL micelles (lanes 19–22, concentration: 5, 20, 50, and 100 µg mL^{-1}) in the dark field (Figure 4d), the mobility of DNA did not show a significant change compared to that of supercoiled DNA (lane 27). These experiments suggested that DNA damage induced by DOX@PolyRuCHL micelles was highly dependent on light irradiation.

Some Ru complexes can cleave DNA or bind to DNA after light irradiation.[28] Photocleavage induced the breakage of DNA single strands and decreased their mobility in gels, resulting in migration from supercoiled DNA (Lane 2) to between linear DNA (Lane 3) and relaxed circular DNA (Lane 4). Photobinding induced by the cross-linking of DNA further decreased its mobility, causing migration above the relaxed circular DNA. Our results demonstrated that red light irradiation promoted crosslinking of DNA with chlorambucil-conjugated Ru complexes (released from PolyRuCHL micelles). The chlorambucil-conjugated Ru complexes increased the DNA-binding ability. The chlorambucil-conjugated Ru complexes and DOX released from DOX@PolyRuCHL micelles synergistically enhanced the damage to DNA. Thus, this synergistic effect could overcome the deactivation pathway caused by enhanced DNA repair capacity in multidrug-resistant tumor cells.[15,43]

2.3. Evaluating the Antitumor Efficiency of DOX@PolyRuCHL in vivo

Encouraged by the effect of DOX@PolyRuCHL on the inhibition of the growth of multidrug-resistant tumor cells in vitro, we further constructed an in vivo multidrug-resistant MCF-7R tumor model in BALB/c nude mice to evaluate the antitumor efficiency of DOX@PolyRuCHL in vivo (**Figure 5**a). Mice were randomly divided into six groups: 1) control group, no treatment, 2) light only group, 3) free DOX group, 4) DOX@PolyRuCHL micelles group, 5) PolyRuCHL micelles + Light irradiation, and 6) DOX@PolyRuCHL micelles + Light irradiation. DOX or the micelles was injected into the central parts of solid tumors, which are hypoxic core regions and have complicated environment to deactivate anticancer effects.[44] Intratumoral injection was a suitable way to demonstrate the efficacy of our system. For the groups that need light irradiation, the tumors were exposed to a 660 nm laser (360 J cm^{-2}) after injection of DOX or the micelles for 4 h. We used this optimized light irradiation condition according to the photosubstitution and the American National Standard for Safe Use of Lasers.[26] Red light focused on the subcutaneous tumor during irradiation. Irradiation at different dosages in our experiment did not result in harm. No overheating was observed.

The tumor volumes of each group were monitored for 12 days (Figure 5b). The tumor volume in the control group increased by ≈18-fold at day 12. Neither light-only treatment (increased by ≈15-fold) nor free DOX treatment (increased by ≈15-fold) showed a significant reduction in tumor growth compared to the control group. The tumor volumes increased to varying degrees after treatment with DOX@PolyRuCHL micelles (increased by ≈10-fold) or PolyRuCHL micelles with light irradiation (increased by ≈3-fold). Conversely, treatment with DOX@PolyRuCHL micelles with light irradiation efficiently retarded tumor growth. On day 12, the mice were sacrificed, and the tumors were isolated for imaging (Figure S12, Supporting Information). The tumor weights in each group showed the same trend as the tumor volumes (Figure 5c), which confirmed that irradiating DOX@PolyRuCHL micelles efficiently inhibited the growth of multidrug-resistant tumors in vivo.

To further evaluate the antitumor efficacy, the tumor tissues were analyzed using hematoxylin and eosin (H&E) staining (Figure 5d). Most cells in the light-only group showed healthy morphology, which demonstrated that red light irradiation was nontoxic. Apoptotic and dead cells increased to varying degrees after tumors were treated with DOX, DOX@PolyRuCHL micelles or DOX@PolyRuCHL micelles + Light. However, large numbers of apoptotic and dead cells were observed in the H&E staining image of the DOX@PolyRuCHL micelles + Light group. Moreover, Ki-67 immunohistochemical (IHC) staining was used to assess tumor cell proliferation (Figure 5e). Light treatment only resulted in limited reductions in Ki-67 expression. DOX, DOX@PolyRuCHL micelles, and PolyRuCHL micelles + Light treatments induced moderate decreases in Ki-67 expression. However, DOX@PolyRuCHL micelles with light irradiation significantly decreased Ki-67 expression in the tumor tissue, demonstrating the higher antitumor activity of DOX@PolyRuCHL micelles under light irradiation.
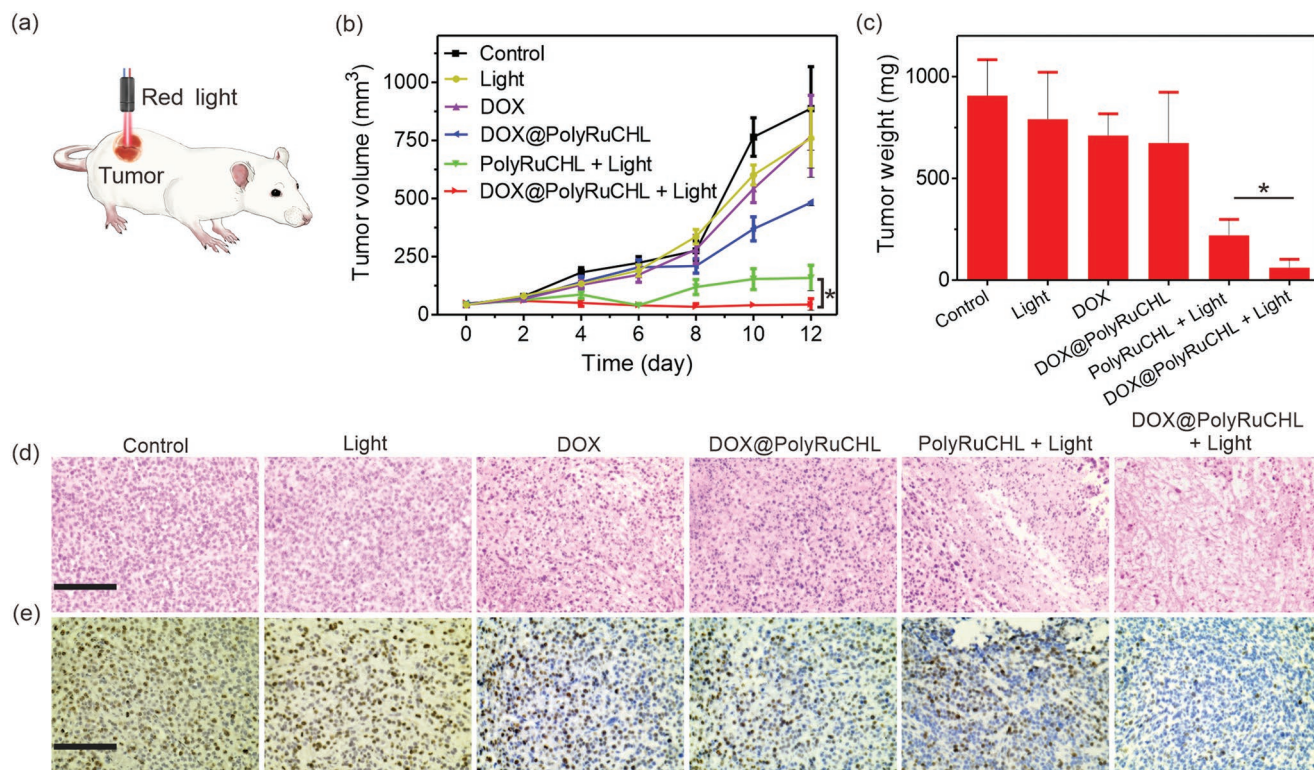
Figure 5. a) Schematic illustration of anticancer phototherapy using DOX@PolyRuCHL micelles in a multidrug-resistant tumor-bearing mouse model. The micelles are activated by red light at the tumor site. b) Tumor volumes for six groups with different treatments for 12 days. Control group: mice, no treatment; Light group: mice exposed to red light irradiation by a 660 nm laser (360 J cm^{-2}); DOX group: mice injected with free DOX; DOX@Poly-RuCHL micelles group: mice injected with DOX@PolyRuCHL micelles; PolyRuCHL micelles + Light group: mice injected with PolyRuCHL micelles and then exposed to red light irradiation by a 660 nm laser (360 J cm^{-2}); DOX@PolyRuCHL micelles + Light group: mice injected with DOX@PolyRuCHL micelles and then exposed to red light irradiation by a 660 nm laser (360 J cm^{-2}). (*$p < 0.05$, two-tailed Student's t-test, $n = 5$). c) Tumor weights for six groups with different treatments at day 12. Mice were sacrificed, and the tumors were isolated for weighing (*$p < 0.05$, $n = 5$). Evaluation of the antitumor efficacy of each treatment modality by histological analysis: d) hematoxylin and eosin (H&E) staining and e) Ki-67 immunohistochemical (IHC) staining of the tumor tissues. Scale bar: 100 µm.

We also evaluated the biocompatibility of DOX@Poly-RuCHL. Hemolysis was studied by incubating DOX@Poly-RuCHL micelles (100–500 µg mL^{-1}) with red blood cells (Figure S13, Supporting Information). No hemolytic effect was observed. Additionally, blood biochemistry data (Figure S14, Supporting Information) revealed that almost all the parameters that represented liver function and kidney functions in the mice were in the normal ranges after treatment with DOX@PolyRuCHL micelles + Light. The treated mice did not show any unusual behavior, and there was no distinct variation in their body weights (Figure S15, Supporting Information). All these experiments demonstrated the good biocompatibility and safety of the treatment.

3. Conclusion

We demonstrated that red-light-responsive DOX@PolyRuCHL micelles reversed multidrug resistance in vitro and in vivo. PolyRuCHL acts as a nanocarrier to deliver DOX into multidrug-resistant cancer cells. By using nanocarriers, the deactivation pathway caused by the overexpressed P-glycoproteins was overcome. In addition, red light irradiation induces the co-release of drug-conjugated Ru complexes and DOX. The co-release inhibits the proliferation of multidrug-resistant cancer cells and has a synergistic effect, because the drug-conjugated Ru complex and DOX cause different types of DNA damage, which overcomes the deactivation pathway caused by DNA repair. We also demonstrated that phototherapy of multidrug-resistant tumors using DOX@PolyRuCHL micelles effectively inhibited tumor growth in vivo. Red-light-induced co-release of both conjugated and encapsulated drugs from nanocarriers represents a new strategy against multidrug-resistant tumors.

4. Experimental Section

Preparation of Micelles: DOX hydrochloride (0.9 mg) was dissolved in DMF (0.1 mL). Three equivalents of trimethylamine were added to the solution to obtain hydrophobic DOX. PolyRuCHL (2.2 mg) was dissolved in 0.3 mL of THF/DMF mixture (v/v = 4/1) and stirred for 10 min. Then, the DOX solution was added to the PolyRuCHL solution, and the mixture was stirred for 20 min. After that, 3.2 mL of Milli-Q water was gently added to the solution, and the solution was stirred for another 20 min. Subsequently, the mixture was purified in a dialysis tube (MWCO 3.5 K) against Milli-Q water for two days to remove the organic solvents. Finally, the solution was collected from the dialysis tube. DOX@PolyRuCHL was in agreement with the definition of micelles. The concentration of DOX

in the micelles was controlled during in the loading process. The amount of DOX encapsulated in the micelles was measured using fluorescence spectroscopy (TIDAS II spectrometer, J&M). The DOX loading content (DLC) was 14.8%. PolyRuCHL micelles without DOX were prepared using the same procedure without adding DOX.

Cell Imaging: The intracellular distribution of free DOX or DOX@PolyRuCHL micelles in MCF-7R cells was detected using confocal laser scanning microscopy. A total of 2×10^4 cells per well were seeded into an eight-well plate (Nunc Lab-Tek, Thermo Fisher, USA) and cultured in RPMI 1640 medium overnight at 37 °C. Then, the medium was washed and incubated with fresh medium containing free DOX or DOX@PolyRuCHL micelles at a final DOX concentration of 10×10^{-6} M for 270 or 120 min, respectively. After that, MCF-7R cells containing DOX@PolyRuCHL micelles were divided into three groups: 1) incubation for another 150 min; 2) after irradiating the cells with 660 nm light for 10 min (30 J cm^{-2}), incubation for another 140 min; and 3) after irradiating the cells with 660 nm light for 30 min (90 J cm^{-2}), incubation for another 120 min. The total incubation time of each group was the same (270 min). Subsequently, the cells were washed using PBS for two times, stained using Hoechst 33 342, and then observed by CLSM. Excitation and detection were performed using CLSM. DOX was excited with a 483 nm laser and detected in the range from 520 to 620 nm. The cell nuclei stained with Hoechst 33342 were excited with a 405 nm laser and detected in the range from 425 to 475 nm.

Cell Viability: The in vitro cytotoxicity/phototoxicity against MCF-7R cells was evaluated by CCK-8 assay. The measurements were conducted calorimetrically by a multireader (TECAN, Infinite M200, Germany) following the manufacturer's protocol and based on the absorbance at 450 nm. The viability of cells was calculated using the following formula: Cell viability (%) = (mean absorbance of treatment group/ mean absorbance of control) × 100%. Specifically, 5×10^3 cells per well were seeded into 96-well plates and incubated for 24 h at 37 °C. Then, the cells were divided into six groups. 1) Control: treatment with the culture medium; 2) Light: treatment with the culture medium for 4 h and then light irradiation for 30 min; 3) DOX@PolyRuCHL micelles: treatment with the culture medium containing various concentrations of DOX@PolyRuCHL micelles; 4) PolyRuCHL micelles + Light group: after treatment with the culture medium containing various concentrations of PolyRuCHL micelles for 4 h, the samples were irradiated for 30 min; 5) DOX@PolyRuCHL micelles + Light group: after treatment with the culture medium containing various concentrations of DOX@PolyRuCHL micelles for 4 h, the samples were irradiated for 30 min; 6) DOX: treatment with the culture medium containing various concentrations of free DOX. An LED at 656 nm (90 J cm^{-2}) was used as the light source. Cell viability was assessed after a terminal incubation time of 24 h.

Gel Electrophoresis Analysis: Plasmid pUC19 amounts were quantified by UV–vis absorption spectroscopy (Lambda 900, Perkin Elmer). Forty micrograms per milliliter of the plasmid was incubated with free DOX, PolyRuCHL micelles, or DOX@PolyRuCHL micelles at various concentrations in 96-well plates. The plasmids containing micelles were incubated for 30 min and then red light activated for 1 h (180 J cm^{-2}) using an LED at 656 nm. Controls were generated by keeping PolyRuCHL micelles or DOX@PolyRuCHL micelles with plasmids in the dark. Then, all the samples were incubated overnight for the same time before gel analysis. To identify the type of damage, linear plasmids and relaxed circle plasmids were prepared and run side-by-side with the experimental samples. Linear plasmids were prepared by digestion with the EcoRI restriction enzyme following the manufacturers' protocol. A relaxed circle plasmid (single cut) was prepared by adding plasmid, dithiothreitol, hydrogen peroxide, and copper phenanthroline into PBS (pH 7.5). The final concentrations of the linear plasmid and the relaxed circle plasmid were both 40 µg mL^{-1}. Samples were resolved on a 1% nonethidium bromide agarose gel and then stained with 0.5 µg mL^{-1} ethidium bromide for 40 min in Tris-acetate buffer followed by destaining for 40 min in Tris-acetate before imaging.

Animal and Tumor Model: BALB/c nude mice (female, 18–20 g, 4–6 weeks) were purchased from Vital River Laboratory Animal Center (Beijing, China). The mice were kept under specific pathogen-free conditions with free access to standard food and water. All protocols for animal studies conformed to the Guide for the Care and Use of Laboratory Animals. All animal experiments were performed in accordance with guidelines approved by the ethics committee of Peking University (Approval No. 2017-Xing-Jie Liang-01).

Antitumor Efficacy in Vivo: MCF-7R cells (1.0×10^7) were inoculated subcutaneously into the flank region of each mouse to establish the tumor-bearing mouse model. When the tumor volume reached ~50 mm^3 after implantation, the mice were split into six groups at random: 1) Control: mice, no treatment; 2) Light: mice exposed to red light irradiation by a 660 nm laser (360 J cm^{-2}); 3) DOX: mice injected with 100 µL free DOX (74 µg mL^{-1}); 4) DOX@PolyRuCHL micelles: mice injected with 100 µL DOX@PolyRuCHL micelles (500 µg mL^{-1}); 5) PolyRuCHL micelles + Light group: mice injected with 100 µL PolyRuCHL micelles (500 µg mL^{-1}) and then exposed to red light irradiation by a 660 nm laser (360 J cm^{-2}); and 6) DOX@PolyRuCHL micelles + Light group: mice injected with 100 µL DOX@PolyRuCHL micelles (500 µg mL^{-1}) and then exposed to red light irradiation by a 660 nm laser (360 J cm^{-2}). The central part of the tumors of mice was directly injected with DOX or micelles on days 1, 3, and 5. After 4 h, the mice were locally irradiated for 30 min in groups (2), (5), and (6), respectively. The weights of the mouse bodies were recorded every 2 days. The tumor volumes were measured using a caliper and calculated as follows: $V = L \times W^2/2$, where L and W were the length and width of the tumor, respectively. On day 12, the tumors of some groups were large. Therefore, the monitor of tumor volumes were stopped on day 12. The mice were sacrificed, and the tumors were collected, weighed and photographed. Paraffin sections of the tumors were subjected to H&E staining and Ki-67 IHC staining at the Beijing Lawke Health Laboratory Center for Clinical Laboratory Development. Images were obtained using a fluorescence microscope (EVOS XL Core, Life Technologies, USA).

Blood Biochemistry Analysis: After all the treatments were finished, blood samples of the mice were collected to detect alkaline phosphatase, aspartate aminotransferase, alanine aminotransferase, uric acid, blood urea nitrogen, serum creatinine, creatine kinase, and total bilirubin by the Beijing Lawke Health Laboratory Center for Clinical Laboratory Development.

Statistical Analysis: Data were presented as the means ± standard deviations (SD). GraphPad Prism 6.0 software (GraphPad Software, Inc., San Diego, CA) was utilized for statistical analyses. The statistical significance of differences between the two groups was determined by two-tailed Student's t-test. $*p < 0.05$ was considered statistically significant.

Supporting Information

Supporting Information is available from the Wiley Online Library or from the author.

Acknowledgements

Conflict of Interest

The authors declare no conflict of interest.

Data Availability Statement

The data that support the findings of this study are available from the corresponding author upon reasonable request.

[1] M. Resistance, in *Encyclopedic Reference of Molecular Pharmacology*, Springer, Berlin, Heidelberg **2004**, p. p. 611.

[2] C. Holohan, S. Van Schaeybroeck, D. B. Longley, P. G. Johnston, *Nat. Rev. Cancer* **2013**, *13*, 714.

[3] J. I. Fletcher, M. Haber, M. J. Henderson, M. D. Norris, *Nat. Rev. Cancer* **2010**, *10*, 147.

[4] J. L. Markman, A. Rekechenetskiy, E. Holler, J. Y. Ljubimova, *Adv. Drug Delivery Rev.* **2013**, *65*, 1866.

[5] W.-H. Chen, G.-F. Luo, W.-X. Qiu, Q. Lei, L.-H. Liu, D.-W. Zheng, S. Hong, S.-X. Cheng, X.-Z. Zhang, *Chem. Mater.* **2016**, *28*, 6742.

[6] L. Tang, Z. Wang, Q. Mu, Z. Yu, O. Jacobson, L. Li, W. Yang, C. Huang, F. Kang, W. Fan, Y. Ma, M. Wang, Z. Zhou, X. Chen, *Adv. Mater.* **2020**, *32*, 2002739.

[7] R. Xing, Q. Zou, C. Yuan, L. Zhao, R. Chang, X. Yan, *Adv. Mater.* **2019**, *31*, 1900822.

[8] L. Qiao, S. Hu, K. Huang, T. Su, Z. Li, A. Vandergriff, J. Cores, P.-U. Dinh, T. Allen, D. Shen, H. Liang, Y. Li, K. Cheng, *Theranostics* **2020**, *10*, 3474.

[9] Z. Ma, J. Li, K. Lin, M. Ramachandran, D. Zhang, M. Showalter, C. De Souza, A. Lindstrom, L. N. Solano, B. Jia, S. Urayama, Y. Duan, O. Fiehn, T.-Y. Lin, M. Li, Y. Li, *Nat. Commun.* **2020**, *11*, 4615.

[10] Y. Zhang, J. Yu, H. N. Bomba, Y. Zhu, Z. Gu, *Chem. Rev.* **2016**, *116*, 12536.

[11] J. Kuang, W. Song, J. Yin, X. Zeng, S. Han, Y.-P. Zhao, J. Tao, C.-J. Liu, X.-H. He, X.-Z. Zhang, *Adv. Funct. Mater.* **2018**, *28*, 1800025.

[12] Y. Cheng, X. Jiao, W. Fan, Z. Yang, Y. Wen, X. Chen, *Biomaterials* **2020**, *256*, 120191.

[13] T. Feng, L. Zhou, Z. Wang, C. Li, Y. Zhang, J. Lin, D. Lu, P. Huang, *Biomaterials* **2020**, *232*, 119709.

[14] T. Wei, C. Chen, J. Liu, C. Liu, P. Posocco, X. Liu, Q. Cheng, S. Huo, Z. Liang, M. Fermeglia, S. Pricl, X.-J. Liang, P. Rocchi, L. Peng, *Proc. Natl. Acad. Sci. USA* **2015**, *112*, 2978.

[15] P. A. Bradbury, M. H. Kulke, R. S. Heist, W. Zhou, C. Ma, W. Xu, A. L. Marshall, R. Zhai, S. M. Hooshmand, K. Asomaning, *Pharmacogen. Genomics* **2009**, *19*, 613.

[16] P. Sun, Q. Deng, L. Kang, Y. Sun, J. Ren, X. Qu, *ACS Nano* **2020**, *14*, 13894.

[17] M. Chen, X. Liang, C. Gao, R. Zhao, N. Zhang, S. Wang, W. Chen, B. Zhao, J. Wang, Z. Dai, *ACS Nano* **2018**, *12*, 7312.

[18] J. Li, J. Huang, Y. Lyu, J. Huang, Y. Jiang, C. Xie, K. Pu, *J. Am. Chem. Soc.* **2019**, *141*, 4073.

[19] Y. Lyu, D. Cui, H. Sun, Y. Miao, H. Duan, K. Pu, *Angew. Chem., Int. Ed.* **2017**, *56*, 9155.

[20] X. Li, J. F. Lovell, J. Yoon, X. Chen, *Nat. Rev. Clin. Oncol.* **2020**, *17*, 657.

[21] C. Li, Y. Zhang, Z. Li, E. Mei, J. Lin, F. Li, C. Chen, X. Qing, L. Hou, L. Xiong, H. Hao, Y. Yang, P. Huang, *Adv. Mater.* **2018**, *30*, 1706150.

[22] L. H. Fu, Y. Wan, C. Li, C. Qi, T. He, C. Yang, Y. Zhang, J. Lin, P. Huang, *Adv. Funct. Mater.* **2021**, 2009848.

[23] W. Sun, S. Li, B. Haupler, J. Liu, S. Jin, W. Steffen, U. S. Schubert, H. J. Butt, X. J. Liang, S. Wu, *Adv. Mater.* **2017**, *29*, 1603702.

[24] W. Sun, Y. Wen, R. Thiramanas, M. Chen, J. Han, N. Gong, M. Wagner, S. Jiang, M. S. Meijer, S. Bonnet, H.-J. Butt, V. Mailänder, X.-J. Liang, S. Wu, *Adv. Funct. Mater.* **2018**, *28*, 1804227.

[25] X. Zeng, Y. Wang, J. Han, W. Sun, H. J. Butt, X. J. Liang, S. Wu, *Adv. Mater.* **2020**, *32*, 2004766.

[26] S. Wu, H. J. Butt, *Adv. Mater.* **2016**, *28*, 1208.

[27] L. Zeng, P. Gupta, Y. Chen, E. Wang, L. Ji, H. Chao, Z.-S. Chen, *Chem. Soc. Rev.* **2017**, *46*, 5771.

[28] E. Wachter, A. Zamora, D. K. Heidary, J. Ruiz, E. C. Glazer, *Chem. Commun.* **2016**, *52*, 10121.

[29] J. D. Knoll, C. Turro, *Coord. Chem. Rev.* **2015**, *282*, 110.

[30] V. T. Huynh, P. de Souza, M. H. Stenzel, *Macromolecules* **2011**, *44*, 7888.

[31] M. Chen, W. Sun, A. Kretzschmann, H.-J. Butt, S. Wu, *J. Inorg. Biochem.* **2020**, *207*, 111052.

[32] S. H. Askes, A. Bahreman, S. Bonnet, *Angew. Chem., Int. Ed.* **2014**, *53*, 1029.

[33] L. N. Lameijer, D. Ernst, S. L. Hopkins, M. S. Meijer, S. H. Askes, S. E. Le Dévédec, S. Bonnet, *Angew. Chem., Int. Ed.* **2017**, *56*, 11549.

[34] L. Zayat, M. G. Noval, J. Campi, C. I. Calero, D. J. Calvo, R. Etchenique, *ChemBioChem* **2007**, *8*, 2035.

[35] C. Xie, W. Sun, H. Lu, A. Kretzschmann, J. Liu, M. Wagner, H.-J. Butt, X. Deng, S. Wu, *Nat. Commun.* **2018**, *9*, 3842.

[36] W. Sun, R. Thiramanas, L. D. Slep, X. Zeng, V. Mailander, S. Wu, *Chem. - Eur. J.* **2017**, *23*, 10832.

[37] B. S. Howerton, D. K. Heidary, E. C. Glazer, *J. Am. Chem. Soc.* **2012**, *134*, 8324.

[38] L. N. Lameijer, S. L. Hopkins, T. G. Brevé, S. H. Askes, S. Bonnet, *Chem. - Eur. J.* **2016**, *22*, 18484.

[39] C. S. Burke, A. Byrne, T. E. Keyes, *J. Am. Chem. Soc.* **2018**, *140*, 6945.

[40] O. Tacar, P. Sriamornsak, C. R. Dass, *J. Pharm. Pharmacol.* **2013**, *65*, 157.

[41] F. A. Fornari, J. K. Randolph, J. C. Yalowich, M. K. Ritke, D. A. Gewirtz, *Mol. Pharmacol.* **1994**, *45*, 649.

[42] R. L. Momparler, M. Karon, S. E. Siegel, F. Avila, *Cancer Res.* **1976**, *36*, 2891.

[43] S. Arora, A. Kothandapani, K. Tillison, V. Kalman-Maltese, S. M. Patrick, *DNA Repair* **2010**, *9*, 745.

[44] J. M. Brown, W. R. Wilson, *Nat. Rev. Cancer* **2004**, *4*, 437.